INSTITUTE OF PLASMA PHYSICS

NAGOYA UNIVERSITY

RESEARCH REPORT

NAGOYA, JAPAN

Coupled Electron-Plasma and Ion Acoustic Solitons Excited by Parametric Instability†

H. Ikezi, K. Nishikawa*,
H. Hojo* and K. Mima*

IPPJ-196 October 1974

Further communication about this report is to be sent to the Research Information Center, Institute of Plasma Physics, Nagoya University, Nagoya, Japan.

---

† Paper to be presented in the Fifth International Conference on Plasma Physics and Controlled Nuclear Fusion Research.

* Permanent address: Faculty of Science, Hiroshima University, Hiroshima, Japan.

Coupled Electron-Plasma and Ion-Acoustic Solitons Excited by Parametric Instability

H. Ikezi,
Institute of Plasma Physics, Nagoya University,
Nagoya, Japan
K. Nishikawa, H. Hojo and K. Mima
Faculty of Science, Hiroshima University,
Hiroshima, Japan

Abstract

Self-modulation of the high-frequency electric field is observed when its frequency is near the electron plasma frequency. The localized field due to the self-modulation is found to make depressions in the plasma density, and to be trapped in the density dip which moves with the ion-acoustic speed. The depth of the dip reaches to 20% of the unperturbed density. The maximum amplitudes of the high-frequency field and the density dip are linearly proportional to each other. All these features are quantitatively explained by the results of the theory of coupled electron-plasma and ion-acoustic solitary waves.

1. Introduction

Parametric instability by an intense high-frequency wave has been considered an important mechanism of plasma heating. Although several experiments have confirmed linear instability theories by observing either enhancement of electrostatic fluctuations[1] or onset of anomalous absorption[2] at theoretically predicted threshold pump intensities, no direct comparison between theory and experiment has been made for the nonlinear saturation state. The present paper reports the theoretical and experimental work on the nonlinear stationary state of the parametric instability of a one-dimensional electron plasma wave. In particular, we have observed a self-modulation of an electron plasma wave and the associated density dip, propagating in unison approximately with the ion-acoustic speed. The result can be explained as coupled electron-plasma and ion-acoustic solitons propagating in the overdense plasma.

2. Observation of Self-Modulation and Formation of Plasma Cavity

An argon plasma is produced by a double plasma source in one end of a cylindrical microwave cavity as shown in Fig.1. Typical plasma parameters are the electron temperature $T_e \simeq 1.5$ eV, the electron density $n \simeq 5 \times 10^9$ cm^{-3}, the ion temperature $T_i \lesssim 0.2$ eV, the argon pressure $p \simeq 2 \times 10^{-4}$ Torr, and the background noise level $\delta n/n_0 \sim 10^{-3}$. An antenna placed at the other end of the cavity excites the dipole mode of frequency $\omega_0/2\pi$ (= 0.64 GHz) in the plasma region. The plasma density is radially nonuniform and the cut-off surface (the surface where $\omega_0 = \omega_{pe}$, the electron plasma frequency) stays inside the plasma as shown by a dotted line in Fig.1. The low-frequency density perturbation is detected by observing the electron saturation current to a Langmuir probe and the high-frequency field by observing the potential difference between two closely spaced wires (1 mm diam. and 5 mm long). The cut-off surface is located by measuring with interferometer a weak pump field which changes its direction, at $\omega = \omega_{pe}$ in a cold plasma model.

Growth of the modulational instability has been observed by applying a stepwise pump power starting at time t = 0. The typical distribution of the plasma density (the electron saturation current to the probe) and of the high-frequency field along the direction of the pump electric field are plotted in Fig.2 for every 1 μsec time interval after turning-on the pump. The plasma density starts decreasing at a place near the cut-off surface; then the density depression expands mainly toward the overdense region with the velocity 2×10^5 cm/sec which is approximately the ion-acoustic velocity. The expanding front eventually forms a stable narrow dip - cavity - in the overdense region and at the same time another dip starts growing at the place where the former dip appeared. This process is repeated, and an oscillatory structure is eventually formed. The depth of the dip reaches about 7% of the unperturbed density.

Figure 2(b) shows the correlation of the self-modulation of the high-frequency field with the density depression. The initial growth rate of the modulation in the unit of the electron plasma period, γ/ω_{pe}, is 3×10^{-4}. The growth rate is approximately proportional to the pump power. At the density dip, the observed field intensity E^2 becomes up to 5 times larger than E_0^2 which is the intensity immediately after turning-on the pump. The envelope of the high-frequency field propagates together with the density perturbation, indicating that the high-frequency field is trapped in the density depression.

3. Theory of Coupled Wave Soliton

We interpret the observed evolution of the wave as follows: First, the ponderomotive force expels the plasma from a region where the electric field is strong and makes a cavity in the plasma, which in turn traps the field and strengthen the ponderomotive force. This process is essentially the oscillating two-stream instability[3] and occurs near the cut-off surface, where the high-frequency field is most efficiently modulated by the density perturbation. Since thus produced density depression has a sharp expanding front, the dispersion effect of the ion-acoustic wave tends to develop oscillation and forms a stationary narrow density dip at the expanding front.

To analyze the observed density dip which traps the electron plasma wave and moves with the ion-acoustic velocity, we consider coupled equations for electron-plasma and ion-acoustic waves[4]. For electron-wave, we use the Schrödinger equation with the potential proportional to the electron density perturbation δn[5]:

$$i \frac{\partial}{\partial t} u + \frac{3}{2} \frac{\partial^2}{\partial x^2} u + (\Delta + \frac{\tilde{n}}{2n_0}) u = 0 \qquad (1)$$

where we used ω_{pe}^{-1} and the Debye length λ_D as units of the time and length, and u denoted the electron fluid velocity as $u \exp(-i\omega_0 t) + u^* \exp(i\omega_0 t)$; $\Delta = (\omega_0^2 - 1)/2$. In the stationary state moving with velocity V, the high-frequency component of the electron fluid velocity, $u_e(x, t)$, can be written as

$$u_e(x, t) = w(\xi) \exp\{-i [\omega_0 - \frac{V^2}{6}] t\} + c.c. \qquad (2)$$

where $\xi = x - x_0 - Vt$, x_0 being the initial position, and $w(\xi)$ satisfies the equation

$$\frac{3}{2} \frac{\partial^2}{\partial \xi^2} w(\xi) + [\Delta - \frac{v(\xi)}{2}] w(\xi) = 0 \qquad (3)$$

Here $v(\xi)$ is the normalized density perturbation, $v = \tilde{n}/n_0$. For ion-waves propagating approximately with the ion-acoustic speed c_s, we can use the Korteweg-deVries equation with the ponderomotive force acting as a source [5]:

$$\frac{1}{\varepsilon}(\frac{\partial}{\partial t} - c_s \frac{\partial}{\partial x}) v + v \frac{\partial}{\partial x} v + \frac{1}{2} \frac{\partial^3}{\partial x^3} v = - \frac{\partial}{\partial x} |u|^2 \qquad (4)$$

where ε^2 is the electron-to-ion mass ratio. The integrated form of this equation is

$$\frac{\partial^2}{\partial \xi^2} v(\xi) - 2\lambda v(\xi) + v^2(\xi) + |w(\xi)|^2 + W = 0 \qquad (5)$$

where $\lambda = (V - c_s)/c_s$, c_s being the square root of the electron-to-ion mass ratio in the present units used in this section, and W is an integration constant.

The coupled equations, (3) and (5), are exactly solved in terms of Jacobi's elliptic functions. As a special case, solitary wave solutions are obtained in the form

$$v(\xi) = 12\Delta \operatorname{sech}^2 \zeta \qquad (6)$$

$$w(\xi) = -(192)^{1/2} \Delta \operatorname{sech}\zeta \tanh\zeta \qquad (7)$$

with

$$\zeta = (-2\Delta/3)^{1/2}\xi, \text{ and } \lambda = 20\Delta/3 \qquad (8)$$

Note that the solitary wave solusion exists only in the overdense region ($\Delta < 0$) and the density perturbation v is negative in the region of large high-frequency field $|w|$, indicating density dip traps the electron plasma wave. From (6) and (7) we find important fact that v is linear in w. This result contrasts with the usual static pressure balance relation $v \propto -|w|^2$.

The ion Landau damping due to a finite ion temperature prevents a sharp resonance at $V = \varepsilon$, $|\lambda|$ $(= |V - \varepsilon|)$ becoming at least of order ν_i/ω_s, where ν_i and ω_s are the damping rate and the frequency of the ion-acoustic wave. On the other hand, a large ion-density perturbation (of order $|v| \sim |w|$) predicted by the present theory assumes $|\lambda|$ to be of order $|w|$ or less; otherwise, $|v|$ becomes much smaller being of order $|w|^2$. This implies that in the case $|w|$ acts as a pump the ion Landau damping brings in a threshold ($|w| > \nu_i/\omega_s$) for the occurrence of a large ion-density perturbation.

4. Experimental Test of Theoretical Results

To test above theoretical results, an experimental set up shown in Fig.3 is employed. The electron temperature in this new device is 3 eV which is higher than the temperature in the previous plasma. Since the ion temperature is the same as the previous one, the Landau damping of the ion-acoustic perturbation due to the ions is reduced. This double plasma system[7] efficiently launches a large-amplitude ion-acoustic wave from the left-hand-side grid into a region where the pump field is applied by a mesh grid.

The distribution of the plasma density is plotted in Fig. 4(a) for every 5 μsec time interval after a rarefaction ion-acoustic wave is launched. No pump field is applied. The figure clearly shows a wave propagating from left to right with the ion-acoustic speed. If we adjust the plasma density in such a way that the electron plasma frequency at the bottom of the rarefaction wave approximately equals the pump frequency (330 MHz) (so that the plasma is overdense), then the pump field produces a very deep density dip like the one shown in Fig.4(b). The dip moves with the ion-acoustic speed, and its depth δn reaches 20 % of the unperturbed density. The field intensity E^2 in the density dip is enhanced up to an order of magnitude larger than the intensity outside the dip, indicating high-frequency field is trapped. The depth δn can be controlled by changing the intensity of the pump field or the width of the launched rarefaction wave.

The relation (6) and (8), which are written as

$$\tilde{n} = -\delta n \, \mathrm{sech}^2\left(\frac{x - c_s t}{D}\right) \qquad (9)$$

$$D/\lambda_D = (18\, n_o/\delta n)^{1/2}$$

in unnormalized unit, predict that the deeper soliton is narrower. We find in Fig.5 that Eq.(9) (solid line) well accounts for the observed relation (dots) between δn and D.

Some detailed features of the high-frequency field have been studied by employing an interferometer. Part of the pump oscillator signal was used as the interferometer reference. Since the dip moves, the time dependent part of the interferometer output indicates phase and amplitude of the trapped wave.

Figure 6(a) shows the density perturbation (middle trace) and the interferometer output (lower trace) which is proportional to the envelope of the trapped field. The dependence of the interferometer signal on the phase of the reference signal showed that the electron plasma wave formed a standing wave in the density dip. In Fig.6(a), the phase of the reference is adjusted in such a way that the maximum interferometer output is obtained. For comparison with the theory, Eqs.(6) and (7) are plotted in Fig.6(b). We can see close similarity in the waveform.

The relation between the depth δn and the maximum electric field E_m is plotted in Fig.7; it clearly indicates a linear relationship between δn and E_m. The theoretically obtained relation

$$\delta n/n_o \sim (E_m^2/16\pi n_o T_e)^{1/2} \qquad (10)$$

agrees with the observed results, indicating the assumption of static pressure balance, $\delta n/n_o \sim E_m^2/16\pi n_o (T_e + T_i)$, is not valid when the low frequency perturbation propagates with the ion-acoustic velocity.

The density dip is formed when the pump intensity exceeds a threshold value given by $|w| = 2(E_o^2/16\pi n_o T_e)^{1/2} \simeq 4 \times 10^{-2}$. Measurements of the spatial damping rate k_i and the wave number k_r gives us the minimum value of γ_i/ω_s $(= k_i/k_r) = 2 \times 10^{-2}$, which is fairly close to $|w|$ at the threshold. This result supports qualitative discussion of the threshold given in the previous section.

All above results have confirmed that the large density dip found in the second device is the coupled electron and ion-acoustic solitary wave which is theoretically obtained in the previous section. The density dip found in the first device also manifests the linear relation between δn and E_m, and the waveform of the trapped field like the one shown in Fig.6. However, it has a width wider than the prediction of (9). This discrepancy can be explained by the ion Landau damping which cut down the large wavenumber components, since T_e/T_i is smaller in the first device.

Finally we note that the large density perturbation generated by modulational instability, which will occur in the Laser-plasma interaction and the other heating experiments, will strongly modify the manner of wave-plasma interaction.

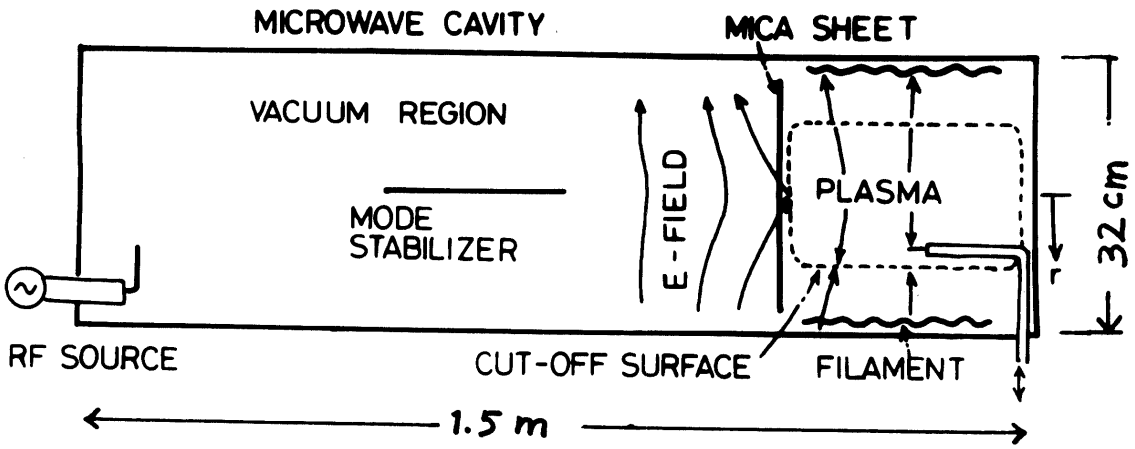

Fig.1. Schematic of the experimental setup. Dotted line indicates the cut-off surface.

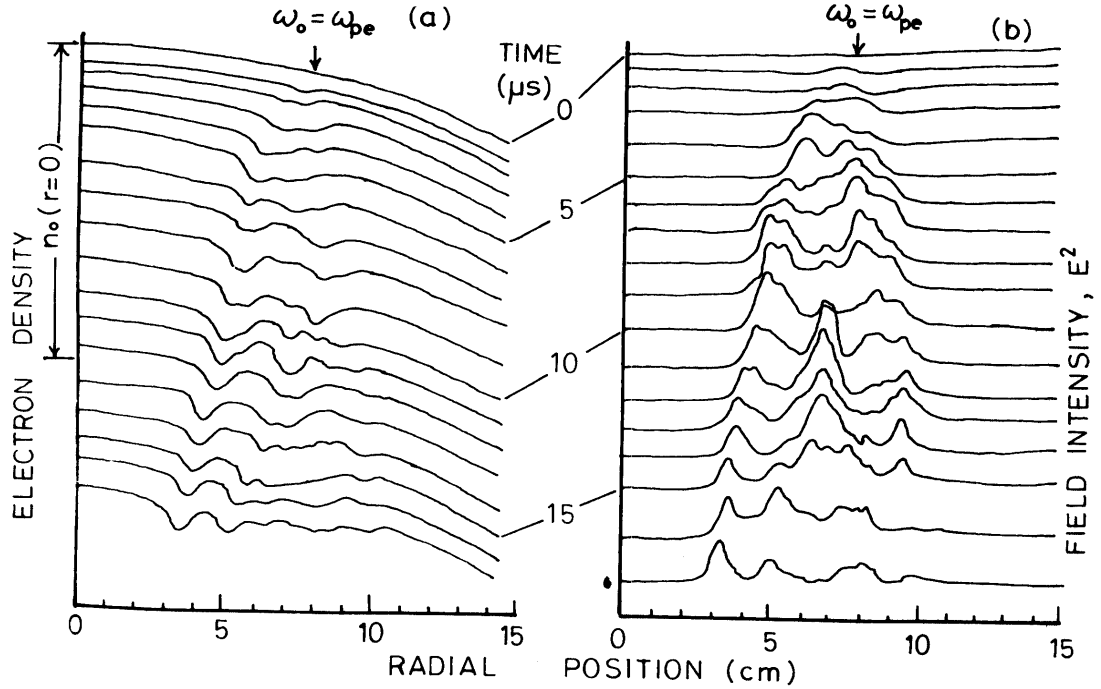

Fig.2. Profile of the density perturbation (a) and the high-frequency field intensity (b). A stepwise pump starts at t = 0. Pump power = 20 W.

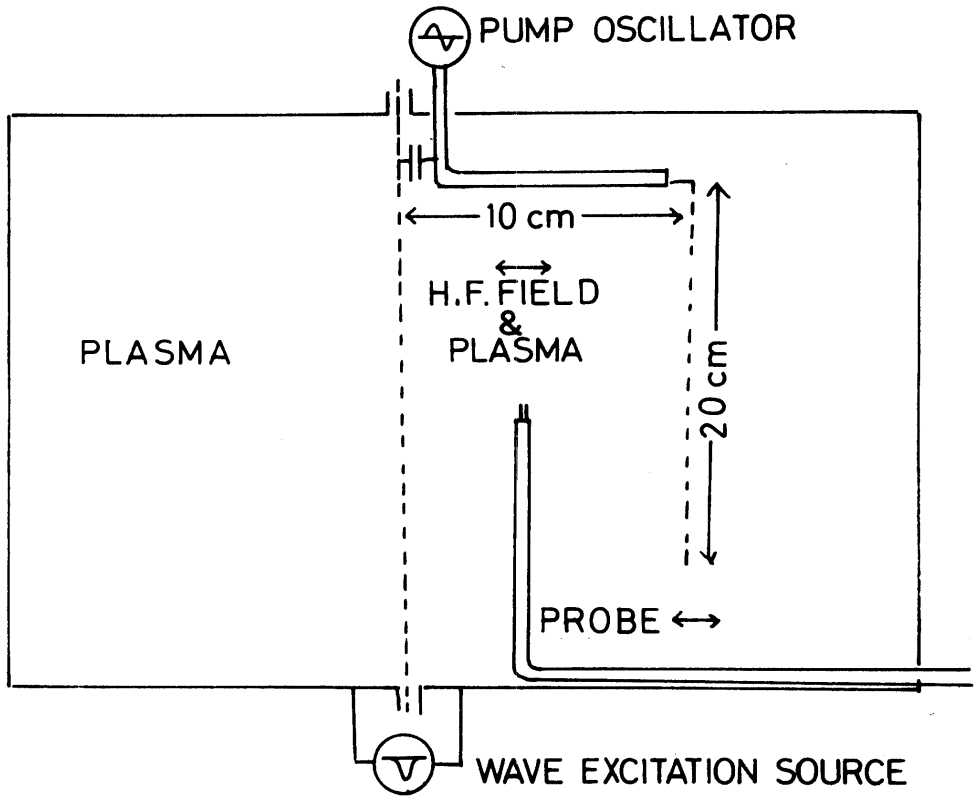

Fig.3. Schematic of the second device.

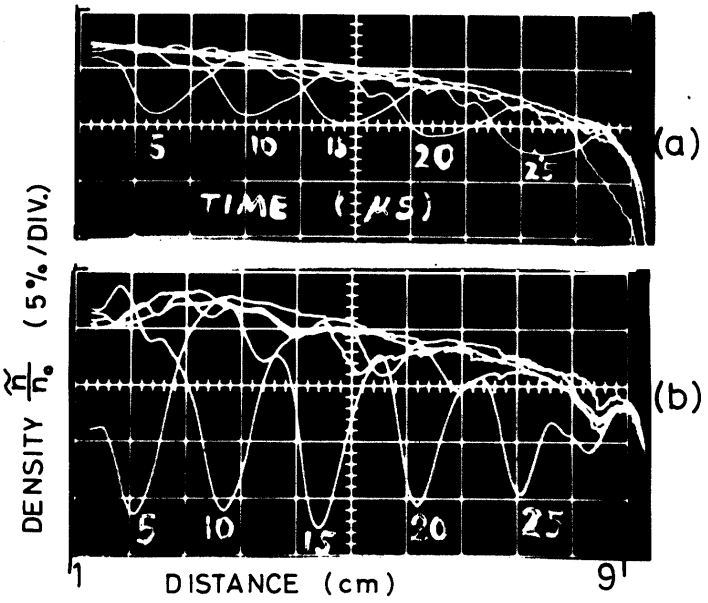

Fig.4. Profile of the density perturbation when a rarefaction wave is launched. (a) No pump. (b) With pump (E_0 = 9 V/cm, $\omega_0/2\pi$ = 330 MHz).

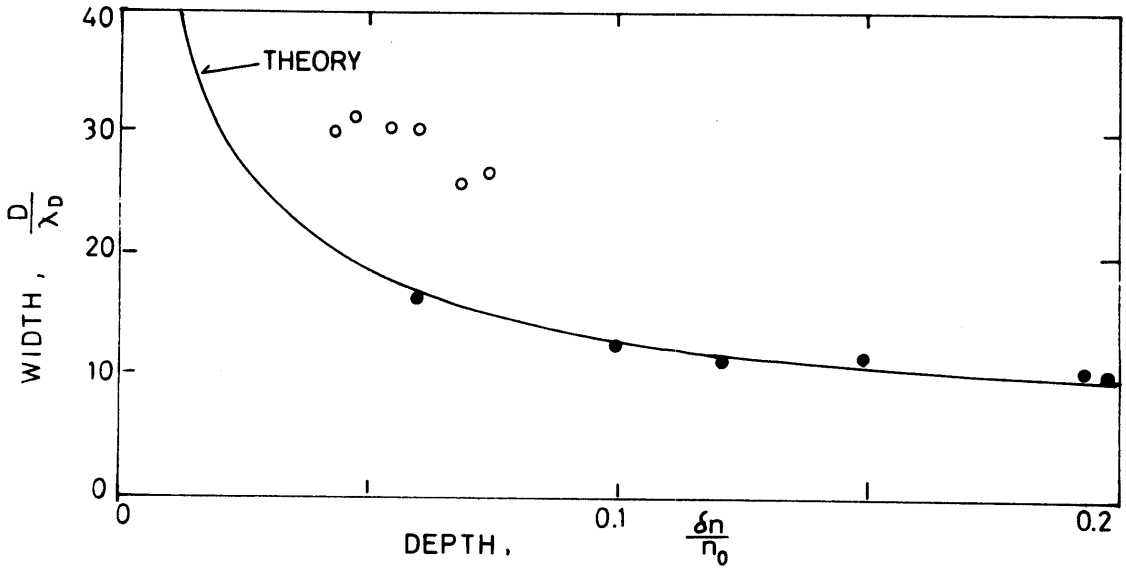

Fig.5. Relation between the depth and the width of the density dip. Circles: data obtained in the first device. Dots: data obtained in the second device.

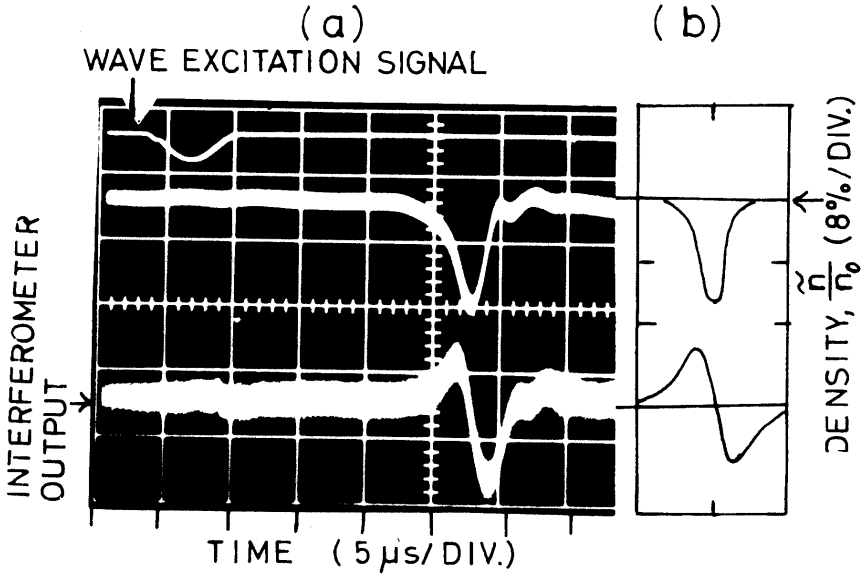

Fig.6. Density perturbation and interferometer output as a function of time. (a) Experimental. (b) Theoretical.

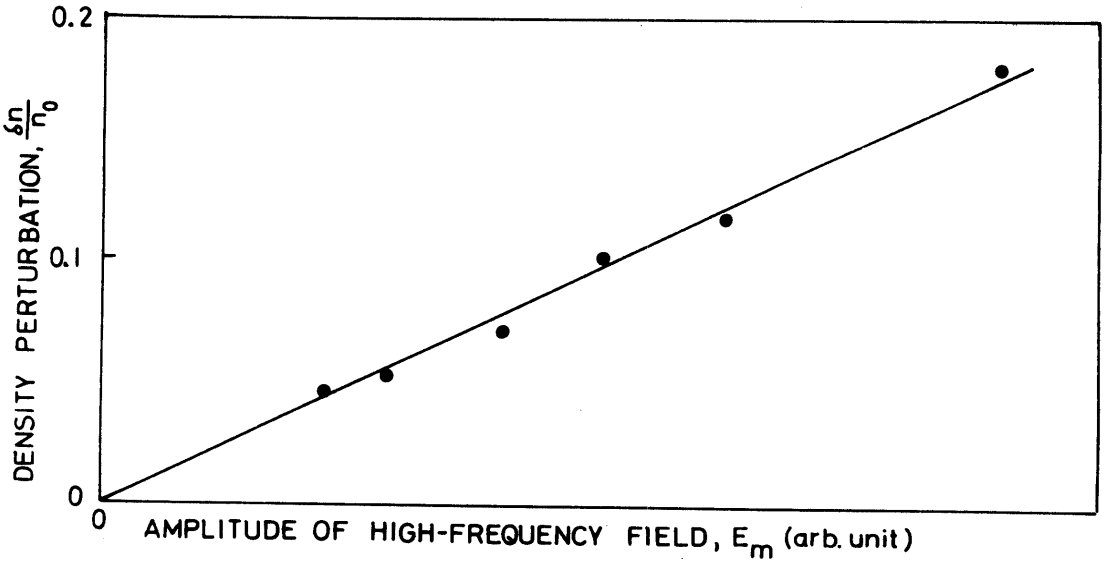

Fig.7. A relation between amplitude of the density perturbation and the high-frequency electric field.